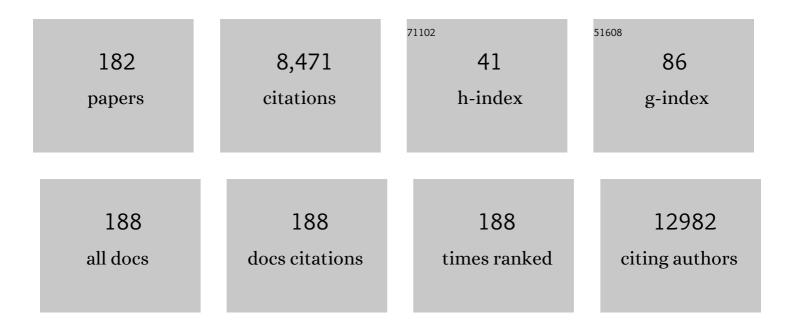
List of Publications by Year in descending order

Source: https://exaly.com/author-pdf/8271174/publications.pdf Version: 2024-02-01



EDIC ABOACVE

#	Article	IF	CITATIONS
1	Guidelines for the welfare and use of animals in cancer research. British Journal of Cancer, 2010, 102, 1555-1577.	6.4	1,167
2	Imaging biomarker roadmap for cancer studies. Nature Reviews Clinical Oncology, 2017, 14, 169-186.	27.6	792
3	Acetyl-CoA Synthetase 2 Promotes Acetate Utilization and Maintains Cancer Cell Growth under Metabolic Stress. Cancer Cell, 2015, 27, 57-71.	16.8	596
4	Malignant transformation alters membrane choline phospholipid metabolism of human mammary epithelial cells. Cancer Research, 1999, 59, 80-4.	0.9	423
5	lmaging early changes in proliferation at 1Âweek post chemotherapy: a pilot study in breast cancer patients with 3â€2-deoxy-3â€2-[18F]fluorothymidine positron emission tomography. European Journal of Nuclear Medicine and Molecular Imaging, 2007, 34, 1339-1347.	6.4	252
6	3'-deoxy-3'-[18F]fluorothymidine as a new marker for monitoring tumor response to antiproliferative therapy in vivo with positron emission tomography. Cancer Research, 2003, 63, 3791-8.	0.9	201
7	Minimally Invasive Pharmacokinetic and Pharmacodynamic Technologies in Hypothesis-Testing Clinical Trials of Innovative Therapies. Journal of the National Cancer Institute, 2006, 98, 580-598.	6.3	189
8	Inhibition of fatty acid desaturation is detrimental to cancer cell survival in metabolically compromised environments. Cancer & Metabolism, 2016, 4, 6.	5.0	186
9	Quantification of Cellular Proliferation in Tumor and Normal Tissues of Patients with Breast Cancer by [18F]Fluorothymidine-Positron Emission Tomography Imaging: Evaluation of Analytical Methods. Cancer Research, 2005, 65, 10104-10112.	0.9	175
10	Positron emission tomography imaging of drug-induced tumor apoptosis with a caspase-3/7 specific [ <sup>18</sup> F]-labeled isatin sulfonamide. Proceedings of the National Academy of Sciences of the United States of America, 2009, 106, 16375-16380.	7.1	157
11	Multiplexed imaging for diagnosis and therapy. Nature Biomedical Engineering, 2017, 1, 697-713.	22.5	133
12	A mathematical-descriptor of tumor-mesoscopic-structure from computed-tomography images annotates prognostic- and molecular-phenotypes of epithelial ovarian cancer. Nature Communications, 2019, 10, 764.	12.8	130
13	Design, Synthesis, and Biological Characterization of a Caspase 3/7 Selective Isatin Labeled with 2-[ <sup>18</sup> F]fluoroethylazide. Journal of Medicinal Chemistry, 2008, 51, 8057-8067.	6.4	126
14	Molecular mechanisms of hypoxia in cancer. Clinical and Translational Imaging, 2017, 5, 225-253.	2.1	119
15	Use of [11C]Choline PET-CT as a Noninvasive Method for Detecting Pelvic Lymph Node Status from Prostate Cancer and Relationship with Choline Kinase Expression. Clinical Cancer Research, 2011, 17, 7673-7683.	7.0	107
16	In vivo evaluation of [18F]fluoroetanidazole as a new marker for imaging tumour hypoxia with positron emission tomography. British Journal of Cancer, 2004, 90, 2232-2242.	6.4	93
17	ICEC0942, an Orally Bioavailable Selective Inhibitor of CDK7 for Cancer Treatment. Molecular Cancer Therapeutics, 2018, 17, 1156-1166.	4.1	93
18	Nm23-transfected MDA-mB-435 human breast carcinoma cells form tumors with altered phospholipid metabolism and pH: A31P nuclear magnetic resonance study in vivo and in vitro. Magnetic Resonance in Medicine, 1999, 41, 897-903.	3.0	91

ERIC ABOAGYE

#	Article	IF	CITATIONS
19	Redistribution of Nucleoside Transporters to the Cell Membrane Provides a Novel Approach for Imaging Thymidylate Synthase Inhibition by Positron Emission Tomography. Cancer Research, 2006, 66, 8558-8564.	0.9	87
20	Alterations of Choline Phospholipid Metabolism in Endometrial Cancer Are Caused by Choline Kinase Alpha Overexpression and a Hyperactivated Deacylation Pathway. Cancer Research, 2014, 74, 6867-6877.	0.9	87
21	<sup>18</sup> F-ICMT-11, a Caspase-3–Specific PET Tracer for Apoptosis: Biodistribution and Radiation Dosimetry. Journal of Nuclear Medicine, 2013, 54, 1551-1556.	5.0	83
22	Modulation of fluorouracil tissue pharmacokinetics by eniluracil: in-vivo imaging of drug action. Lancet, The, 2000, 355, 2125-2131.	13.7	78
23	Antibody Fragment and Affibody ImmunoPET Imaging Agents: Radiolabelling Strategies and Applications. ChemMedChem, 2018, 13, 2466-2478.	3.2	77
24	Pharmacokinetic Evaluation of N-[2-(Dimethylamino)Ethyl]Acridine-4-Carboxamide in Patients by Positron Emission Tomography. Journal of Clinical Oncology, 2001, 19, 1421-1429.	1.6	76
25	Monitoring Predominantly Cytostatic Treatment Response with <sup>18</sup> F-FDG PET. Journal of Nuclear Medicine, 2009, 50, 97S-105S.	5.0	75
26	Gold Nanostar Substrates for Metal-Enhanced Fluorescence through the First and Second Near-Infrared Windows. Chemistry of Materials, 2017, 29, 6916-6926.	6.7	72
27	In vivo Biological Activity of the Histone Deacetylase Inhibitor LAQ824 Is detectable with 3′-Deoxy-3′-[18F]Fluorothymidine Positron Emission Tomography. Cancer Research, 2006, 66, 7621-7629.	0.9	68
28	68Ga-DOTATATE PET/CT parameters predict response to peptide receptor radionuclide therapy in neuroendocrine tumours. Radiotherapy and Oncology, 2019, 141, 108-115.	0.6	62
29	Multi-modal Learning from Unpaired Images: Application to Multi-organ Segmentation in CT and MRI. , 2018, , .		61
30	A bioorthogonal <sup>68</sup> Ga-labelling strategy for rapid in vivo imaging. Chemical Communications, 2014, 50, 9557-9560.	4.1	60
31	Lapatinib access into normal brain and brain metastases in patients with Her-2 overexpressing breast cancer. EJNMMI Research, 2015, 5, 30.	2.5	60
32	Discovery of pre-therapy 2-deoxy-2-18F-fluoro-D-glucose positron emission tomography-based radiomics classifiers of survival outcome in non-small-cell lung cancer patients. European Journal of Nuclear Medicine and Molecular Imaging, 2019, 46, 455-466.	6.4	59
33	Evaluation of Deuterated 18F- and 11C-Labeled Choline Analogs for Cancer Detection by Positron Emission Tomography. Clinical Cancer Research, 2012, 18, 1063-1072.	7.0	58
34	Altered Tissue 3′-Deoxy-3′-[18F]Fluorothymidine Pharmacokinetics in Human Breast Cancer following Capecitabine Treatment Detected by Positron Emission Tomography. Clinical Cancer Research, 2009, 15, 6649-6657.	7.0	52
35	Reproducibility of [11C]Choline-Positron Emission Tomography and Effect of Trastuzumab. Clinical Cancer Research, 2010, 16, 4236-4245.	7.0	52
36	Apparent Diffusion Coefficient of Normal Abdominal Organs and Bone Marrow From Whole-Body DWI at 1.5 T: The Effect of Sex and Age. American Journal of Roentgenology, 2015, 205, 242-250.	2.2	52

#	Article	IF	CITATIONS
37	Positron Emission Tomography Imaging of Tumor Cell Metabolism and Application to Therapy Response Monitoring. Frontiers in Oncology, 2016, 6, 44.	2.8	49
38	[11C]Choline Positron Emission Tomography in Estrogen Receptor–Positive Breast Cancer. Clinical Cancer Research, 2009, 15, 5503-5510.	7.0	48
39	Temporal and Spatial Evolution of Therapy-Induced Tumor Apoptosis Detected by Caspase-3–Selective Molecular Imaging. Clinical Cancer Research, 2013, 19, 3914-3924.	7.0	48
40	Use of radiolabelled choline as a pharmacodynamic marker for the signal transduction inhibitor geldanamycin. British Journal of Cancer, 2002, 87, 783-789.	6.4	46
41	Synthesis and in vitro evaluation of [18F]fluoroethyl triazole labelled [Tyr3]octreotate analogues using click chemistry. Bioorganic and Medicinal Chemistry Letters, 2011, 21, 3122-3127.	2.2	44
42	Noninvasive imaging of cell proliferation following mitogenic extracellular kinase inhibition by PD0325901. Molecular Cancer Therapeutics, 2008, 7, 3112-3121.	4.1	43
43	Targeting Somatostatin Receptors: Preclinical Evaluation of Novel <sup>18</sup> F-Fluoroethyltriazole-Tyr <sup>3</sup> -Octreotate Analogs for PET. Journal of Nuclear Medicine, 2011, 52, 1441-1448.	5.0	41
44	A Novel Radiotracer to Image Glycogen Metabolism in Tumors by Positron Emission Tomography. Cancer Research, 2014, 74, 1319-1328.	0.9	38
45	[18F]Fluoromethyl-[1,2-2H4]-Choline: A Novel Radiotracer for Imaging Choline Metabolism in Tumors by Positron Emission Tomography. Cancer Research, 2009, 69, 7721-7728.	0.9	37
46	Radiosynthesis and pre-clinical evaluation of [18F]fluoro-[1,2-2H4]choline. Nuclear Medicine and Biology, 2011, 38, 39-51.	0.6	37
47	Intratumoral conversion of 5-fluorocytosine to 5-fluorouracil by monoclonal antibody-cytosine deaminase conjugates: noninvasive detection of prodrug activation by magnetic resonance spectroscopy and spectroscopic imaging. Cancer Research, 1998, 58, 4075-8.	0.9	37
48	The Physiological Environment in Cancer Vascularization, Invasion and Metastasis. Novartis Foundation Symposium, 2008, 240, 23-45.	1.1	36
49	The HDAC6 inhibitor C1A modulates autophagy substrates in diverse cancer cells and induces cell death. British Journal of Cancer, 2018, 119, 1278-1287.	6.4	36
50	Detection of tumor response to chemotherapy by 1H nuclear magnetic resonance spectroscopy: effect of 5-fluorouracil on lactate levels in radiation-induced fibrosarcoma 1 tumors. Cancer Research, 1998, 58, 1063-7.	0.9	36
51	Extraction of 5-fluorouracil by tumor and liver: a noninvasive positron emission tomography study of patients with gastrointestinal cancer. Cancer Research, 2001, 61, 4937-41.	0.9	36
52	Imaging Pharmacodynamics of the α-Folate Receptor–Targeted Thymidylate Synthase Inhibitor BGC 945. Cancer Research, 2008, 68, 3827-3834.	0.9	35
53	New Frontiers in the Design and Synthesis of Imaging Probes for PET Oncology: Current Challenges and Future Directions. Molecular Imaging and Biology, 2012, 14, 653-666.	2.6	35
54	Clinical Translation of a Click-Labeled <sup>18</sup> F-Octreotate Radioligand for Imaging Neuroendocrine Tumors. Journal of Nuclear Medicine, 2016, 57, 1207-1213.	5.0	35

#	Article	IF	CITATIONS
55	Significant metal enhanced fluorescence of Ag <sub>2</sub> S quantum dots in the second near-infrared window. Nanoscale, 2016, 8, 12869-12873.	5.6	35
56	Clinical translation of [18F]ICMT-11 for measuring chemotherapy-induced caspase 3/7 activation in breast and lung cancer. European Journal of Nuclear Medicine and Molecular Imaging, 2018, 45, 2285-2299.	6.4	35
57	Use of positron emission tomography in anticancer drug development. Investigational New Drugs, 2003, 21, 169-181.	2.6	33
58	Lactic acidosis induces resistance to the pan-Akt inhibitor uprosertib in colon cancer cells. British Journal of Cancer, 2020, 122, 1298-1308.	6.4	32
59	The novel choline kinase inhibitor ICL-CCIC-0019 reprograms cellular metabolism and inhibits cancer cell growth. Oncotarget, 2016, 7, 37103-37120.	1.8	32
60	Fully automatic, multiorgan segmentation in normal whole body magnetic resonance imaging ( <scp>MRI</scp> ), using classification forests ( <scp>CF</scp> s), convolutional neural networks ( <scp>CNN</scp> s), and a multiâ€atlas ( <scp>MA</scp> ) approach. Medical Physics, 2017, 44, 5210-5220.	3.0	31
61	Integrated analysis of multiple receptor tyrosine kinases identifies Axl as a therapeutic target and mediator of resistance to sorafenib in hepatocellular carcinoma. British Journal of Cancer, 2019, 120, 512-521.	6.4	31
62	Improved radiosynthesis of the apoptosis marker 18F-ICMT11 including biological evaluation. Bioorganic and Medicinal Chemistry Letters, 2011, 21, 6945-6949.	2.2	30
63	Fluorescence enhancement from single gold nanostars: towards ultra-bright emission in the first and second near-infrared biological windows. Nanoscale, 2018, 10, 15854-15864.	5.6	30
64	Towards multiplexed near-infrared cellular imaging using gold nanostar arrays with tunable fluorescence enhancement. Nanoscale, 2019, 11, 2079-2088.	5.6	30
65	Real-time measurements of cellular oxygen consumption, pH, and energy metabolism using nuclear magnetic resonance spectroscopy. Magnetic Resonance in Medicine, 2001, 45, 749-755.	3.0	29
66	Preclinical Assessment of Carboplatin Treatment Efficacy in Lung Cancer by 18F-ICMT-11-Positron Emission Tomography. PLoS ONE, 2014, 9, e91694.	2.5	29
67	Kinetic filtering of [ <sup>18</sup> F]Fluorothymidine in positron emission tomography studies. Physics in Medicine and Biology, 2010, 55, 695-709.	3.0	27
68	Development and Evaluation of an <sup>18</sup> F-Radiolabeled Monocyclam Derivative for Imaging CXCR4 Expression. Molecular Pharmaceutics, 2019, 16, 2106-2117.	4.6	26
69	Radiological assessment of Peritoneal Cancer Index on preoperative CT in ovarian cancer is related to surgical outcome and survival. Radiologia Medica, 2020, 125, 770-776.	7.7	26
70	Choline Kinase Alpha (CHKα) as a Therapeutic Target in Pancreatic Ductal Adenocarcinoma: Expression, Predictive Value, and Sensitivity to Inhibitors. Molecular Cancer Therapeutics, 2016, 15, 323-333.	4.1	25
71	Snapshot imprinting: rapid identification of cancer cell surface proteins and epitopes using molecularly imprinted polymers. Nano Today, 2021, 41, 101304.	11.9	24
72	Positron Emission Tomography Imaging of Small Animals in Anticancer Drug Development. Molecular Imaging and Biology, 2005, 7, 53-58.	2.6	23

#	Article	IF	CITATIONS
73	Microwave gallium-68 radiochemistry for kinetically stable bis(thiosemicarbazone) complexes: structural investigations and cellular uptake under hypoxia. Dalton Transactions, 2016, 45, 144-155.	3.3	23
74	Preclinical evaluation of a CXCR4-specific 68Ga-labelled TN14003 derivative for cancer PET imaging. Bioorganic and Medicinal Chemistry, 2014, 22, 796-803.	3.0	22
75	Preclinical Evaluation of 3- <sup>18</sup> F-Fluoro-2,2-Dimethylpropionic Acid as an Imaging Agent for Tumor Detection. Journal of Nuclear Medicine, 2014, 55, 1506-1512.	5.0	22
76	AKT activation controls cell survival in response to HDAC6 inhibition. Cell Death and Disease, 2016, 7, e2286-e2286.	6.3	22
77	Bioorthogonal chemistry for <sup>68</sup> Ga radiolabelling of DOTAâ€containing compounds. Journal of Labelled Compounds and Radiopharmaceuticals, 2014, 57, 291-297.	1.0	21
78	Multicenter Reproducibility of 18F-Fluciclatide PET Imaging in Subjects with Solid Tumors. Journal of Nuclear Medicine, 2015, 56, 1855-1861.	5.0	21
79	Cancer Research UK procedures in manufacture and toxicology of radiotracers intended for Pre-phase I positron emission tomography studies in cancer patients. British Journal of Cancer, 2002, 86, 1052-1056.	6.4	20
80	Targeting autophagy sensitises lung cancer cells to Src family kinase inhibitors. Oncotarget, 2018, 9, 27346-27362.	1.8	20
81	Highlights lecture EANM 2016: "Embracing molecular imaging and multi-modal imaging: a smart move for nuclear medicine towards personalized medicine― European Journal of Nuclear Medicine and Molecular Imaging, 2017, 44, 1559-1574.	6.4	19
82	Mn–salen catalysed benzylic C–H activation for the synthesis of aryl [ <sup>18</sup> F]CF <sub>3</sub> -containing PET probes. Chemical Communications, 2015, 51, 8439-8441.	4.1	18
83	Novel Approach to Imaging Active Takayasu Arteritis Using Somatostatin Receptor Positron Emission Tomography/Magnetic Resonance Imaging. Circulation: Cardiovascular Imaging, 2020, 13, e010389.	2.6	18
84	2-Substituted-2,3-dihydro-1H-quinolin-4-ones via Acid-Catalyzed Tandem Rupe Rearrangement-Donnelly-Farrell Ring Closure of 2-(3′-HydroxyÂpropynyl)anilines. Synlett, 2011, 2011, 241-244.	1.8	17
85	Imaging of cellular proliferation in liver metastasis by [18F]fluorothymidine positron emission tomography: effect of therapy. Physics in Medicine and Biology, 2012, 57, 3419-3433.	3.0	17
86	Recommendations for measurement of tumour vascularity with positron emission tomography in early phase clinical trials. European Radiology, 2012, 22, 1465-1478.	4.5	17
87	Exploiting altered patterns of choline kinase-alpha expression on human prostate tissue to prognosticate prostate cancer. Journal of Clinical Pathology, 2015, 68, 703-709.	2.0	17
88	3D Growth of Cancer Cells Elicits Sensitivity to Kinase Inhibitors but Not Lipid Metabolism Modifiers. Molecular Cancer Therapeutics, 2019, 18, 376-388.	4.1	17
89	Use of radioiodine in nuclear medicine—A brief overview. Journal of Labelled Compounds and Radiopharmaceuticals, 2021, 64, 92-108.	1.0	17
90	A comparison of machine learning methods for predicting recurrence and death after curative-intent radiotherapy for non-small cell lung cancer: Development and validation of multivariable clinical prediction models. EBioMedicine, 2022, 77, 103911.	6.1	17

ERIC ABOAGYE

#	Article	IF	CITATIONS
91	Validation analysis of the novel imaging-based prognostic radiomic signature in patients undergoing primary surgery for advanced high-grade serous ovarian cancer (HGSOC). British Journal of Cancer, 2022, 126, 1047-1054.	6.4	17
92	Synthesis and evaluation of nucleoside radiotracers for imaging proliferation. Nuclear Medicine and Biology, 2012, 39, 652-665.	0.6	16
93	Design of symmetrical and nonsymmetrical N,N-dimethylaminopyridine derivatives as highly potent choline kinase alpha inhibitors. MedChemComm, 2013, 4, 693.	3.4	16
94	Small Organ Segmentation in Whole-Body MRI Using a Two-Stage FCN and Weighting Schemes. Lecture Notes in Computer Science, 2018, , 346-354.	1.3	16
95	Chemistry Considerations for the Clinical Translation of Oncology PET Radiopharmaceuticals. Molecular Pharmaceutics, 2020, 17, 2245-2259.	4.6	15
96	Radiopharmaceuticals as probes to characterize tumour tissue. European Journal of Nuclear Medicine and Molecular Imaging, 2015, 42, 537-561.	6.4	14
97	Altered cytochrome 2E1 and 3A P450â€dependent drug metabolism in advanced ovarian cancer correlates to tumourâ€associated inflammation. British Journal of Pharmacology, 2019, 176, 3712-3722.	5.4	14
98	PET Imaging of Steroid Hormone Receptor Expression. Molecular Imaging, 2015, 14, 7290.2015.00026.	1.4	13
99	Synthesis, Radiolabelling and In Vitro Imaging of Multifunctional Nanoceramics. ChemNanoMat, 2018, 4, 361-372.	2.8	13
100	Development of <sup>68</sup> Ga-labelled ultrasound microbubbles for whole-body PET imaging. Chemical Science, 2019, 10, 5603-5615.	7.4	13
101	[18F]FET-βAC-TOCA: The Design, Evaluation and Clinical Translation of a Fluorinated Octreotide. Cancers, 2020, 12, 865.	3.7	13
102	The application of radiomics in laryngeal cancer. British Journal of Radiology, 2021, 94, 20210499.	2.2	13
103	Discovery of a biomarker candidate for surgical stratification in high-grade serous ovarian cancer. British Journal of Cancer, 2021, 124, 1286-1293.	6.4	13
104	Luciferase fragment complementation imaging in preclinical cancer studies. Oncoscience, 2014, 1, 310-325.	2.2	13
105	Preparation of the iodine-124 derivative of the Bolton-Hunter reagent ([124I]I-SHPP) and its use for labelling a VEGF antibody as a PET tracer. Journal of Labelled Compounds and Radiopharmaceuticals, 2002, 45, 1077-1090.	1.0	12
106	18F-labelling of a cyclic pentapeptide inhibitor of the chemokine receptor CXCR4. Journal of Fluorine Chemistry, 2012, 135, 200-206.	1.7	12
107	Design and synthesis of novel 18F-radiolabelled glucosamine derivatives for cancer imaging. MedChemComm, 2013, 4, 653.	3.4	12
108	Epigenetic changes in gastroenteropancreatic neuroendocrine tumours. Oncogene, 2015, 34, 4439-4447.	5.9	12

#	Article	IF	CITATIONS
109	[18F]Fluciclatide PET as a biomarker of response to combination therapy of pazopanib and paclitaxel in platinum-resistant/refractory ovarian cancer. European Journal of Nuclear Medicine and Molecular Imaging, 2020, 47, 1239-1251.	6.4	12
110	The Oxford Classic Links Epithelial-to-Mesenchymal Transition to Immunosuppression in Poor Prognosis Ovarian Cancers. Clinical Cancer Research, 2021, 27, 1570-1579.	7.0	12
111	Preclinical development and current status of the fluorinated 2-nitroimidazole hypoxia probe N-(2-hydroxy-3,3,3-trifluoropropyl)-2-(2-nitro-1-imidazolyl) acetamide (SR 4554, CRC 94/17): a non-invasive diagnostic probe for the measurement of tumor hypoxia by magnetic resonance spectroscopy and imaging, and by positron emission tomography. Anti-cancer Drug Design, 1998, 13, 703-30.	0.3	12
112	Repeatability of quantitative 18F-FLT uptake measurements in solid tumors: an individual patient data multi-center meta-analysis. European Journal of Nuclear Medicine and Molecular Imaging, 2018, 45, 951-961.	6.4	11
113	Reliability of dynamic contrast-enhanced magnetic resonance imaging data in primary brain tumours: a comparison of Tofts and shutter speed models. Neuroradiology, 2019, 61, 1375-1386.	2.2	11
114	An improved automated radiosynthesis of [ <sup>18</sup> F]FET-βAG-TOCA. Reaction Chemistry and Engineering, 2019, 4, 569-574.	3.7	11
115	3-D Microvascular Imaging Using High Frame Rate Ultrasound and ASAP Without Contrast Agents: Development and Initial <i>In Vivo</i> Evaluation on Nontumor and Tumor Models. IEEE Transactions on Ultrasonics, Ferroelectrics, and Frequency Control, 2019, 66, 939-948.	3.0	11
116	Introduction to the National Cancer Imaging Translational Accelerator (NCITA): a UK-wide infrastructure for multicentre clinical translation of cancer imaging biomarkers. British Journal of Cancer, 2021, 125, 1462-1465.	6.4	11
117	The future of imaging: developing the tools for monitoring response to therapy in oncology: the 2009 Sir James MacKenzie Davidson Memorial lecture. British Journal of Radiology, 2010, 83, 814-822.	2.2	10
118	Transcriptional analysis of multiple ovarian cancer cohorts reveals prognostic and immunomodulatory consequences of ERV expression. , 2021, 9, e001519.		10
119	Synthesis of [18F]fluoro-pivalic acid: an improved PET imaging probe for the fatty acid synthesis pathway in tumours. MedChemComm, 2013, 4, 1350.	3.4	9
120	Scavenging strategy for specific activity improvement: application to a new CXCR4â€specific cyclopentapeptide positron emission tomography tracer. Journal of Labelled Compounds and Radiopharmaceuticals, 2013, 56, 679-685.	1.0	9
121	Evaluation of apoptosis imaging biomarkers in a genetic model of cell death. EJNMMI Research, 2019, 9, 18.	2.5	9
122	One-Pot Radiosynthesis and Biological Evaluation of a Caspase-3 Selective 5-[123,1251]iodo-1,2,3-triazole derived Isatin SPECT Tracer. Scientific Reports, 2019, 9, 19299.	3.3	9
123	Spatial heterogeneity of radiolabeled choline positron emission tomography in tumors of patients with non-small cell lung cancer: first-in-patient evaluation of [ <sup>18</sup> F]fluoromethyl-(1,2- <sup>2</sup> H <sub>4</sub> )-choline. Theranostics, 2020, 10, 8677-8690.	10.0	9
124	Monitoring Response to Transarterial Chemoembolization in Hepatocellular Carcinoma Using <sup>18</sup> F-Fluorothymidine PET. Journal of Nuclear Medicine, 2020, 61, 1743-1748.	5.0	9
125	Hypoxic cell cytotoxin tirapazamine induces acute changes in tumor energy metabolism and pH:A31p magnetic resonance spectroscopy study. Radiation Oncology Investigations, 1998, 6, 249-254.	0.9	8
126	Design, synthesis and initial characterisation of a radiolabelled [ <sup>18</sup> F]pyrimidoindolone probe for detecting activated caspase-3/7. Organic and Biomolecular Chemistry, 2015, 13, 5418-5423.	2.8	8

#	Article	IF	CITATIONS
127	Synthesis and pre-clinical evaluation of a [18F]fluoromethyl-tanaproget derivative for imaging of progesterone receptor expression. RSC Advances, 2016, 6, 57569-57579.	3.6	8
128	Depicting Changes in Tumor Biology in Response to Cetuximab Monotherapy or Combination Therapy by Apoptosis and Proliferation Imaging Using <sup>18</sup> F-ICMT-11 and <sup>18</sup> F-FLT PET. Journal of Nuclear Medicine, 2018, 59, 1558-1565.	5.0	8
129	Tracing Nutrient Flux Following Monocarboxylate Transporter-1 Inhibition with AZD3965. Cancers, 2020, 12, 1703.	3.7	8
130	Radiolabelling an <sup>18</sup> F biologic <i>via</i> facile IEDDA "click―chemistry on the GE FASTLab™ platform. Reaction Chemistry and Engineering, 2021, 6, 1070-1078.	3.7	8
131	Correction of Fat-Water Swaps in Dixon MRI. Lecture Notes in Computer Science, 2016, , 536-543.	1.3	8
132	Evaluation of lactate as a 1H nuclear magnetic resonance spectroscopy index for noninvasive prediction and early detection of tumor response to radiation therapy in EMT6 tumors. Radiation Research, 1998, 150, 38-42.	1.5	8
133	Iodo Silanes as Superior Substrates for the Solid Phase Synthesis of Molecularly Imprinted Polymer Nanoparticles. Polymers, 2022, 14, 1595.	4.5	8
134	lodination of terminal alkynes using KI/CuSO4 – A facile method with potential for radio-iodination. Tetrahedron Letters, 2019, 60, 936-939.	1.4	7
135	Development of a fluorine-18 radiolabelled fluorescent chalcone: evaluated for detecting glycogen. EJNMMI Radiopharmacy and Chemistry, 2020, 5, 17.	3.9	7
136	Integrating the OHIF Viewer into XNAT: Achievements, Challenges and Prospects for Quantitative Imaging Studies. Tomography, 2022, 8, 497-512.	1.8	7
137	Development of a multi-task learning V-Net for pulmonary lobar segmentation on CT and application to diseased lungs. Clinical Radiology, 2022, 77, e620-e627.	1.1	7
138	Clinical Translation of Molecular Imaging Agents Used in PET Studies of Cancer. Advances in Cancer Research, 2014, 124, 329-374.	5.0	6
139	Histogram analysis of apparent diffusion coefficient from whole-body diffusion-weighted MRI to predict early response to chemotherapy in patients with metastatic colorectal cancer: preliminary results. Clinical Radiology, 2018, 73, 832.e9-832.e16.	1.1	6
140	Solid-supported cyanoborohydride cartridges for automation of reductive amination radiochemistry. Reaction Chemistry and Engineering, 2019, 4, 1748-1751.	3.7	6
141	Clinical translation of 18F-fluoropivalate – a PET tracer for imaging short-chain fatty acid metabolism: safety, biodistribution, and dosimetry in fed and fasted healthy volunteers. European Journal of Nuclear Medicine and Molecular Imaging, 2020, 47, 2549-2561.	6.4	6
142	Caspase-Based PET for Evaluating Pro-Apoptotic Treatments in a Tuberculosis Mouse Model. Molecular Imaging and Biology, 2020, 22, 1489-1494.	2.6	6
143	Fully automated deep-learning section-based muscle segmentation from CT images for sarcopenia assessment. Clinical Radiology, 2022, 77, e363-e371.	1.1	6
144	Imaging as a pharmacodynamic and response biomarker in cancer. Clinical and Translational Imaging, 2014, 2, 13-31.	2.1	5

#	Article	IF	CITATIONS
145	Effective Detection and Monitoring of Glioma Using [18F]FPIA PET Imaging. Biomedicines, 2021, 9, 811.	3.2	5
146	Consideration of Metabolite Efflux in Radiolabelled Choline Kinetics. Pharmaceutics, 2021, 13, 1246.	4.5	5
147	2′-Deoxy-2′,2′-difluorothymidine analogues for radiolabeling with fluorine-18 and other biomedical applications. Tetrahedron Letters, 2015, 56, 3293-3297.	1.4	4
148	Baseline and longitudinal variability of normal tissue uptake values of [ 18 F]-fluorothymidine-PET images. Nuclear Medicine and Biology, 2017, 51, 18-24.	0.6	4
149	Detecting hypoxia <i>in vitro</i> using <sup>18</sup> F-pretargeted IEDDA "click―chemistry in live cells. RSC Advances, 2021, 11, 20335-20341.	3.6	4
150	Phosphorylation Status of Thymidine Kinase 1 Following Antiproliferative Drug Treatment Mediates 3′-Deoxy-3′-[18F]-Fluorothymidine Cellular Retention. PLoS ONE, 2014, 9, e101366.	2.5	4
151	Imaging in drug development. Clinical Advances in Hematology and Oncology, 2006, 4, 902-4.	0.3	4
152	Towards an MMP-2-activated molecular agent for cancer imaging. Dalton Transactions, 2018, 47, 1530-1534.	3.3	3
153	Optimal method for metabolic tumour volume assessment of cervical cancers with inter-observer agreement on [18F]-fluoro-deoxy-glucose positron emission tomography with computed tomography. European Journal of Nuclear Medicine and Molecular Imaging, 2021, 48, 2009-2023.	6.4	3
154	A kit-based aluminium-[ <sup>18</sup> F]fluoride approach to radiolabelled microbubbles. Chemical Communications, 2021, 57, 11677-11680.	4.1	3
155	Direct incorporation of [18F] into Aliphatic Systems: A promising Mn-catalysed Labelling Technique for PET Imaging. Current Radiopharmaceuticals, 2021, 14, 101-106.	0.8	3
156	Phosphatidylcholine metabolic transformation and progression signature as a pharmacodynamic biomarker. Oncotarget, 2010, 1, 163-6.	1.8	3
157	A multifractal approach to spaceâ€filling recovery for PET quantification. Medical Physics, 2014, 41, 112505.	3.0	2
158	Metabolically active tumour volume segmentation from dynamic [18F]FLT PET studies in non-small cell lung cancer. EJNMMI Research, 2015, 5, 26.	2.5	2
159	Identification of ABC Transporter Interaction of a Novel Cyanoquinoline Radiotracer and Implications for Tumour Imaging by Positron Emission Tomography. PLoS ONE, 2016, 11, e0161427.	2.5	2
160	Evaluation of 18F-fluorothymidine positron emission tomography ([18F]FLT-PET/CT) methodology in assessing early response to chemotherapy in patients with gastro-oesophageal cancer. EJNMMI Research, 2016, 6, 81.	2.5	2
161	Multi-frame rate plane wave contrast-enhanced ultrasound imaging for tumour vascular imaging and perfusion quantification. , 2017, , .		2
162	Novel Non-Congeneric Derivatives of the Choline Kinase Alpha Inhibitor ICL-CCIC-0019. Pharmaceutics, 2021, 13, 1078.	4.5	2

ERIC ABOAGYE

#	Article	IF	CITATIONS
163	68Ga-DOTATATE PET/CT to predict response to peptide receptor radionuclide therapy (PRRT) in neuroendocrine tumours (NETs) Journal of Clinical Oncology, 2017, 35, 4093-4093.	1.6	2
164	Variational Bayes for high-dimensional proportional hazards models with applications within gene expression. Bioinformatics, 2022, 38, 3918-3926.	4.1	2
165	Functional imaging of hepatocellular carcinoma. Hepatic Oncology, 2016, 3, 137-153.	4.2	1
166	Contrast vs Non-Contrast Enhanced Microvascular Imaging Using Acoustic Sub-Aperture Processing (ASAP): In Vivo Demonstration. , 2018, , .		1
167	High-Contrast 3D in Vivo Microvascular Imaging Using Scanning 2D Ultrasound and Acoutic Sub-Aperture Processing (ASAP). , 2018, , .		1
168	Synthesis and evaluation of 3′-[ <sup>18</sup> F]fluorothymidine-5′-squaryl as a bioisostere of 3′-[ <sup>18</sup> F]fluorothymidine-5′-monophosphate. RSC Advances, 2021, 11, 12423-12433.	3.6	1
169	Nm23â€transfected MDAâ€mBâ€435 human breast carcinoma cells form tumors with altered phospholipid metabolism and pH: A 31P nuclear magnetic resonance study in vivo and in vitro. Magnetic Resonance in Medicine, 1999, 41, 897-903.	3.0	1
170	Design and Development of Probes forIn vivo Molecular and Functional Imaging of Cancer and Cancer Therapies by Positron Emission Tomography (PET). , 0, , 1243-1270.		1
171	Abstract 4235: Choline metabolism is an early predictor of EGFR-mediated survival in NSCLC. Cancer Research, 2016, 76, 4235-4235.	0.9	1
172	Investigating CXCR4 expression of tumor cells and the vascular compartment: A multimodal approach. PLoS ONE, 2021, 16, e0260186.	2.5	1
173	Multi-frame rate plane wave contrast-enhance ultrasound imaging for tumour vasculature imaging and perfusion quantification. , 2017, , .		Ο
174	Resistance to tyrosine kinase-targeted therapy in lung cancer: Autophagy and metabolic changes. Meta Gene, 2018, 17, S10.	0.6	0
175	Reliability of DCE MRI data in primary brain tumours: a comparison of Tofts and Shutter Speed Models. Neuro-Oncology, 2019, 21, iv11-iv11.	1.2	Ο
176	IMAGING OF PHARMACODYNAMIC END POINTS IN CLINICAL TRIALS. , 2006, , 299-336.		0
177	Abstract A222: Assessment of tumor response to therapy with the caspaseâ€3/7 specific [18F]ICMTâ€11 PET imaging tracer. , 2009, , .		Ο
178	Abstract 5274: Noninvasive early assessment of tumor response to the SMAC mimetic TL32711 with a caspase-3/7-specific PET imaging radiotracer. , 2011, , .		0
179	Abstract 2660: Regulation of 18F-fluorothymidine uptake by thymidine kinase 1 protein phosphorylation , 2013, , .		0
180	Abstract A15: HDAC6 inhibitor C1A abrogates the recruitment of the autophagic machinery and synergizes with proteasome, src kinase, and PI3K-mTOR inhibition , 2013, , .		0

#	Article	IF	CITATIONS
181	Abstract B140: Positron emission tomography imaging of HER2 expression and pharmacodynamic response to HSP90 inhibition with the next-generation ZHER2:2891 Affibody molecule [18F]GE-226 , 2013, , .		Ο
182	Abstract P5-01-02: Evaluation of apoptosis in breast cancer using the novel PET probe [18F]ICMT-11 in patients treated with neoadjuvant FEC chemotherapy: Initial assessment of optimum imaging time and relation to caspase-3 immunostaining. , 2015, , .		0